

## Analysis of capacitance of a cryogenic by-pass line for SIS100 particle accelerator at FAIR

ŁUKASZ TOMKÓW<sup>1,2</sup>, STANISŁAW TROJANOWSKI<sup>3</sup>, MARIAN CISZEK<sup>1,3</sup>,  
MACIEJ CHOROWSKI<sup>1</sup>

<sup>1</sup> *Wrocław University of Technology  
Wyb. Wyspiańskiego 27, 50-370 Wrocław, Poland*

<sup>2</sup> *Joint Institute for Nuclear Research  
Joliot-Curie 6, 141980 Dubna, Russia*

<sup>3</sup> *Institute of Low Temperature and Structure Research  
ul. Okólna 2, 50-422 Wrocław, Poland  
e-mail: lukasz.tomkow@pwr.edu.pl*

(Received: 20.03.2018, revised: 23.07.2018)

**Abstract:** Safety and operation efficiency of the particle accelerators strongly depend on the quality of the supplied electric current and is affected by the electric properties of all elements of the circuit. In this paper the capacitance of the superconducting bus-bars applied in the cryogenic by-pass line for the SIS100 particle accelerator at FAIR is analysed. The unit capacitance of the bus-bars is calculated numerically and found experimentally. A 2D numerical model of a cross-section of the cable is applied. The capacitance is found with three methods. The stored energy, electric displacement field and charge gathered on the surfaces of the device are calculated and analysed. The obtained values are consistent. Experimental measurements are performed using the resonance method. The measuring system is undamped using a negative conductance converter. Small discrepancies are observed between numerical and experimental results. The obtained values are within the requirements of the accelerator design.

**Key words:** line capacitance, superconducting bus-bars, particle accelerators

### 1. Introduction

Quality of current delivered to the superconducting magnets plays crucial role in the behaviour of a particle accelerator. Any disturbances cause deformation of the orbits of the accelerated particles [1] leading to defocusing or even loss of the beam. High energy particles which are off the track can violently interact with the material of the vacuum tube leading to the damage of the equipment [2]. Sometimes the required precision is in order of parts per million. General

international standards of power quality and immunity do not always sufficiently cover the quality demands of a sensitive scientific equipment [3].

At SIS100, by-pass lines will carry liquid helium and electric current between the sections of the accelerator. Six lines will be applied, each with length of approximately 45 m, giving the total length of 270 m [4]. Therefore, electric parameters of the lines will have a significant impact in the context of the accelerator circuit. The lines are designed, manufactured and commissioned by Wrocław University of Technology as the part of the Polish in-kind contribution to the FAIR project. Additional description of the role and construction of by-pass lines in the context of the accelerator and the applied Nuclotron-type cables is presented in our previous paper [5]. In this paper the description of analysis line capacitance is presented. The values of capacitance are measured experimentally and calculated numerically.

## 2. Methods

### 2.1. Calculation of capacitance

In the line assembly two superconducting bus-bars will be placed in a steel tube to ensure proper electrical and thermal shielding [6, 7]. The geometry of the line is presented in Figure 1. The steel tube has a diameter of 28 mm, each bus-bar – 8 mm. The distance between the bus-bars is maintained using G10 spacers and can be adjusted. The remainder is evacuated to generate vacuum for thermal insulation. Capacitance is calculated for several cases representing possible interactions between conducting elements. The obtained values are used further to find capacitances occurring in the actual system. Boundary conditions for each case are shown in Figure 1. The effect of changing a distance between the axes of the cables is analysed.

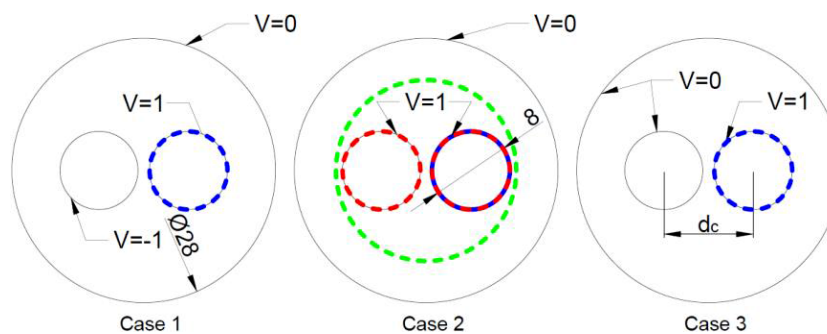


Fig. 1. Cases modelled to find capacitance of the line. Integration paths are marked. The values of potential are given in volts. In case 2: blue – charge and displacement method for a single line; for two lines: green – displacement field method; red – charge method

To calculate the value of capacitance of the entire line the presence of spacers must be considered. Figure 2 presents the example of the longitudinal cross-section of the line with dimensions marked.

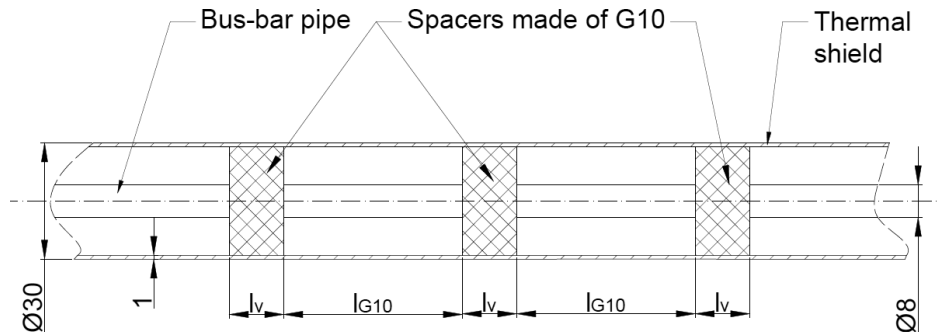


Fig. 2. Cross-section of the analysed superconducting line (all dimensions given in mm)

To find the final value of capacitance in each case or to compare the results obtained with different configuration of spacers an effective electric permittivity  $\varepsilon_{\text{eff}}$  has to be calculated. It is done with Formula (1).

$$\varepsilon_{\text{eff}} = \frac{l_v + \varepsilon_{\text{G10}} \cdot l_{\text{G10}}}{l_v + l_{\text{G10}}} \quad (1)$$

$l_v$  denotes the length of the section surrounded by vacuum and  $l_{\text{G10}}$ , surrounded by G10.  $\varepsilon_{\text{G10}}$  is relative permittivity of G10. To find the actual values of capacitance the numerical results should be multiplied by  $\varepsilon_{\text{eff}}$ . To compare the experimental results obtained with different configurations of spacers the results should be reduced to the capacitance of fully evacuated line by dividing them by  $\varepsilon_{\text{eff}}$ . In the case of measurements presented in this paper this value is 1.685, while for the results described at [9] it is 1.89.

The equivalent circuit of the line with the values of the capacitance marked is presented in Figure 3.  $C_{12}$  represents the capacitance between lines 1 and 2.  $C_{13}$  and  $C_{23}$  are capacitances between a line and the screen.

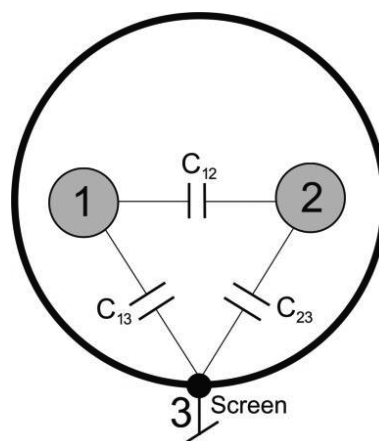


Fig. 3. Equivalent circuit of the analyzed superconducting line

$C_{12}$ ,  $C_{13}$  and  $C_{23}$  are related with capacitances  $C_1$ ,  $C_2$  and  $C_3$  (calculated numerically for respective cases) by Formulas (2), (3) and (4). Formula (2) is derived from the fact that in case 1 the calculated value is  $C_{12}$  connected in parallel with series connection of  $C_{13}$  and  $C_{23}$ .

$$C_1 = C_{12} + \frac{1}{2}C_{13}. \quad (2)$$

In case 2  $C_{13}$  and  $C_{23}$  are connected in parallel, expressed with Formula (3).

$$C_2 = 2C_{13} = 2C_{23}. \quad (3)$$

Formula (4) describes the situation in which  $C_{12}$  and  $C_{13}$  are connected in parallel.

$$C_3 = C_{12} + C_{13}. \quad (4)$$

Since there are 3 formulas and only 2 variables, the values are self-locking and thus it is possible to check the correctness of numerical calculations.

The calculations are performed in Comsol for the region of dielectric assumed as vacuum. The interior of the lines and shell are thus neglected. "Electric Currents" interface of Comsol's AC/DC package is applied. The simulations are done in stationary regime with the values of electric potentials fixed on the surfaces according to Figure 1. In the figure dashed lines mark integration paths for each case. Case 1 reflects the actual operation of the accelerator with opposite potentials on each cable and grounded external tube. Case 2 is used to find components of total capacitance, it will not appear in reality. In this case both cables have the same potential. Here the calculations can be performed for a single or both lines simultaneously. In case 3 one of the cables is grounded. This case is also analyzed only for the purpose of calculation of total capacitance.

Due to the linear symmetry of the considered line a 2D geometry is applied. With such assumptions the calculations are very fast, therefore a very dense mesh is applied with the element size in the range of 0.14–0.3 mm. The calculations are performed for the vacuum region and, as shown later, recalculated for the entire line. Three methods were used to find capacitance in each case. The first method is energy-based. The total energy stored in electric field per unit length  $W_e$  is calculated by integrating energy density over the entire region of dielectric  $S_D$  according to Formula (5).

$$W_e = \iint_{S_D} w_e \, dx \, dy. \quad (5)$$

In this formula  $w_e$  is the volumetric density of electromagnetic energy found with Equation (6).

$$w_e = \frac{\varepsilon}{2} |\mathbf{E}|^2. \quad (6)$$

$\varepsilon$  is the permittivity of the medium found as  $\varepsilon_r \cdot \varepsilon_0$ , where  $\varepsilon_r$  is the relative permittivity of the medium and  $\varepsilon_0$  is the permittivity of vacuum.  $|\mathbf{E}|$  is the module of the electric field calculated as the gradient of electric potential (Formula (7)).

$$\mathbf{E} = -\nabla V. \quad (7)$$

The amount of energy stored in a capacitor  $W_e$  is related to capacitance  $C$  according to Formula (8).

$$W_e = \frac{1}{2}CU^2. \quad (8)$$

In this formula  $U$  is the difference of potential between conductors. In case 1 the difference is 2 V, in cases 2 and 3 it is 1 V. These values are the same for each method.

Second method is based on the integration of electric displacement field  $\mathbf{D}$ . The path of integration  $l$  in cases 1 and 3 and single line calculations in case 2 correspond with the surface of the conductor with positive potential. In the calculation of two conductors in case 2 it surrounds both of them as seen in Figure 1.  $\mathbf{D}$  is found with Formula (9).

$$\mathbf{D} = \varepsilon \mathbf{E}. \quad (9)$$

In this method capacitance is calculated with Formula (10).

$$C = \frac{\oint_l |\mathbf{D}| dl}{U}. \quad (10)$$

Third method is based on charge definition of capacitance expressed with Formula (11).

$$C = \frac{|Q|}{U}. \quad (11)$$

Charge  $Q$  is found with Formula (12).

$$Q = \int_l \rho_s dl. \quad (12)$$

$\rho_s$  is the surface density of electric the charge calculated with Formula (13).  $l$ , in case 2, is the edge of two cables if capacitance is found for both lines and the edge of one cable, if capacitance is calculated for a single line.  $\mathbf{n}$  is the vector normal to the surface of the cable.

$$\rho_s = -\mathbf{n} \cdot \mathbf{D}. \quad (13)$$

## 2.2. Experimental measurements

The experimental measurements were performed at Institute of Low Temperature and Structure Research (INTiBS) [8] and GSI [9]. This paper is based on the experimental results obtained in INTiBS and the applied method is described in this section. The analyzed piece of line has a length of 1 m and contains 30 pieces of G10. The separation between cables ( $d_c$ ) is 9.9 mm. Its general scheme is presented in Figure 4, along with the photography presenting the end of the cable with two Nuclotron type cables, external tube and G10 spacer visible.

The experimental procedure consists of measuring capacitance between three pairs of terminals, analogous to the cases described in the previous section. Unlike in numerical calculations the effect of ends has to be considered and eliminated to obtain meaningful results. To do that the scheme from Figure 3 is modified by adding capacitance  $C_e$  representing the additional capacitance coming from the ends. The circuit with additional capacitance is shown in Figure 5.

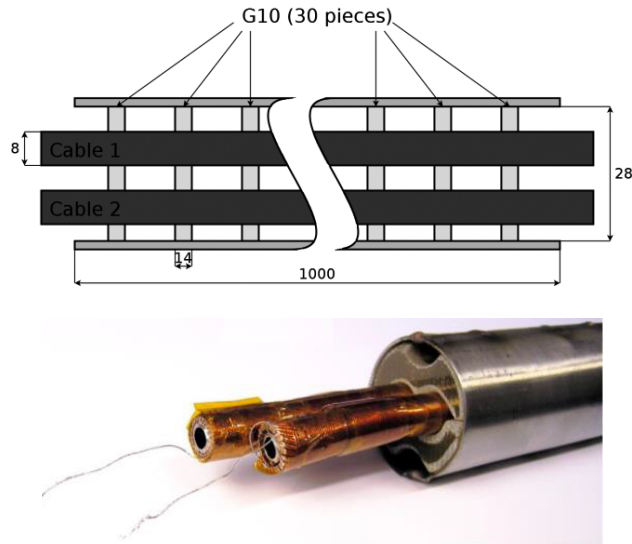


Fig. 4. Scheme and photography of the analyzed line

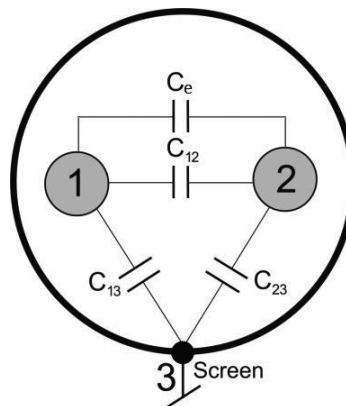


Fig. 5. Equivalent circuit of the analysed superconducting line considering the effect of the ends of the cable

Since the line is assumed to be symmetrical the condition  $C_{13} = C_{23}$  can be applied. With these assumptions Formulas (14) and (15) can be derived.  $C_{m12}$  and  $C_{m13}$  represent measured values.

$$C_{m12} = C_{12} + C_e + C_{13}/2 = C^* + C_{13}/2, \quad (14)$$

$$C_{m13} = \frac{(C_{12} + C_e) \cdot C_{13}}{C_{12} + C_e + C_{13}} + C_{13} = \frac{C^* \cdot C_{13}}{C^* + C_{13}} + C_{13} \cdot \quad (15)$$

In these formulas  $C^*$  is described with Equation (16).

$$C^* = C_{12} + C_e . \quad (16)$$

After solving the set of Equations (14) and (15) for  $C^*$  Formula (17) is obtained.

$$C^* = \frac{4C_{m12} - 2C_{m13}}{4C_{m12} - C_{m13}} \cdot C_{m12} . \quad (17)$$

$C_e$  can be found by summing up capacitances of ends of the line outside of the shielding tube, as described with Formula (18).

$$C_e = C_{l12} + C_{r12} . \quad (18)$$

$C_{l12}$  and  $C_{r12}$  represent the capacitances of the left and right cables. They are found with Formula (19), analogical for both values.

$$C_{l12} = C_{0l12} \cdot l_{l12} . \quad (19)$$

With  $C_{0l12}$  representing the unit capacitance calculated with analytical Formula (20) and  $l_{l12}$  being the length of the fragment of the cable outside the shielding pipe.

$$C_{0l12} = \frac{2.5 \cdot 10^6}{c^2 \cdot \text{arch}\zeta} . \quad (20)$$

$c$  is there the speed of light in vacuum and  $\zeta$  is found with Formula (21), where  $r_c$  is the radius of the cable.

$$\zeta = \frac{d_c}{2r_c} . \quad (21)$$

To measure capacitances  $C_{m12}$  and  $C_{m13}$  the resonance method is applied. The base formula in this method is the following (14):

$$f_r = \frac{1}{2\pi\sqrt{LC}} . \quad (22)$$

$f_r$  is the resonant frequency of the system and  $L$  is its inductance. This formula is valid when the dependence between current and voltage is linear, which is the case with the considered line. In order to find the parameters of the system two measurements have to be performed. The first one is done to find the resonant frequency  $f_{r0}$  of an  $LC$  circuit with known parameters of elements – capacitance  $C_0$  and inductance  $L_0$ . Then measured capacity  $C_1$  is connected to the circuit and resonant frequency  $f_{r1}$  is measured. The considered circuits are presented in Figure 6.

To calculate  $C_1$  based on the measured values of resonant frequencies Formula (23) is applied.

$$C_1 = C_0 \left[ \left( \frac{f_{r0}}{f_{r1}} \right)^2 - 1 \right] . \quad (23)$$

To obtain the accurate value of  $C_1$ , inductance  $L_0$  and capacitance  $C_0$  should be constant throughout the entire measurement. The temperature of the circuit should be maintained on the same level and temperature coefficients of capacitance and inductance should be close to 0.

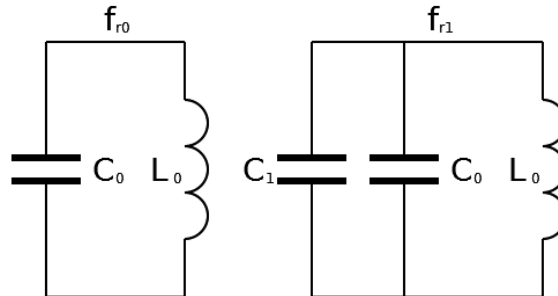


Fig. 6. The idea of resonant frequency method for the measurement of capacitance

The resonant circuit should not be loaded by the measuring devices. In the actual circuit losses occur, especially in the form of Joule heating of coil winding. The undamping parameters have to be found. The circuit can be represented as serial connection of  $R_s$  and  $L_s$ , being resistance and inductance at of the coil at resonant frequency and capacitance  $C$ . At resonant frequency the circuit can be transformed into parallel one  $R_p$  and  $L_p$ . The circuits are presented in Figure 7.

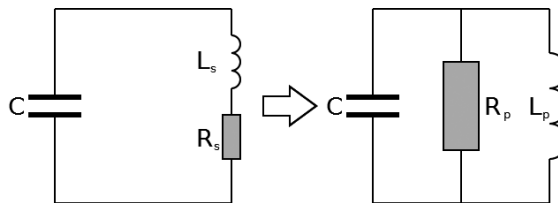


Fig. 7. Transformation of serial representation of a resonant circuit into a parallel one

To transform  $R_s$  and  $L_s$  into  $R_p$  and  $L_p$  Formulas (24) and (25) are applied.

$$R_p = R_s + \frac{\omega^2 L_s^2}{R_s}, \quad (24)$$

$$L_p = L_s + \frac{R_s^2}{\omega^2 L_s}. \quad (25)$$

$\omega$  is calculated with Formula (26).

$$\omega = \omega_0 \sqrt{1 - R_s^2 \frac{C}{L_s}}. \quad (26)$$

Here  $\omega_0 = 2\pi f_s$ . To undamp such a circuit, a negative resistance has to be connected with module  $R_p$ , according to Formula (27).

$$R_p > |-R^*|. \quad (27)$$

$-R^*$  is the negative resistance brought to the circuit by the negative conductance converter. The applied measuring circuit including the converter is presented in Figure 8.



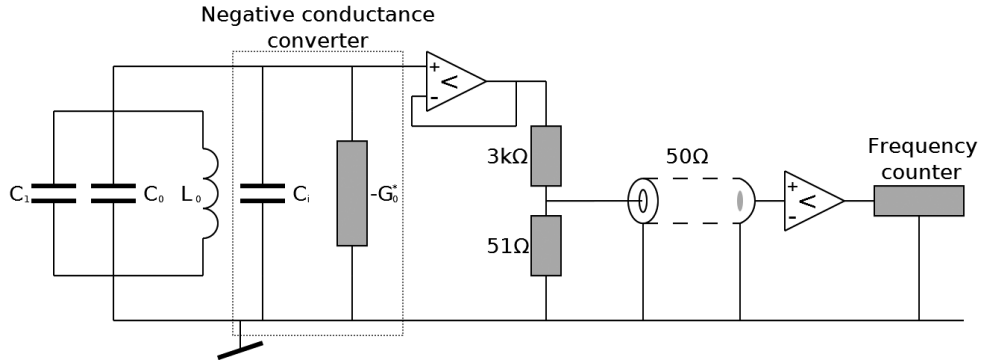


Fig. 8. Applied measuring circuit

$-G^*$  is equal to  $-1/R^*$  found according to the previously described procedure.

The idea of a negative conductance converter is presented in Figure 9. Using it the measuring circuit is undamped until non-decaying oscillations with stable frequency appear. The measurements of  $C$  were performed considering the effect of parasitic capacitance of the converter.

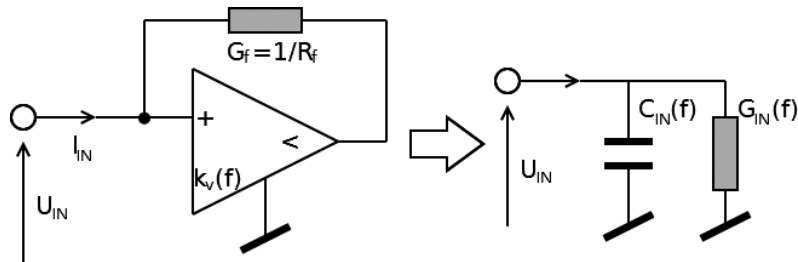


Fig. 9. Idea of negative conductance converter and equivalent circuit

### 3. Results and discussion

The example results of the calculation of an electric displacement field in each case are presented in Figure 10. The field is the strongest in case 1, due to the largest potential difference. It is the weakest in case 2 – the potential difference is low and the wall with zero potential is farther than the distance between cables. The distribution in case 3 is similar to case 1, but the field is weaker as only a single cable exhibits the electric potential.

The corresponding results of the calculations of capacitance for each case, using different methods, for  $d_c$  of 9.5 mm, are gathered in Table 1. They are very similar to each other, showing the consistence of the applied calculation methods.

By substituting the numerically calculated values in Formulas (11), (12) and (13) it is possible to further check the consistence of the numerical results and to find  $C_{12}$ ,  $C_{13}$  and  $C_{23}$ . The results

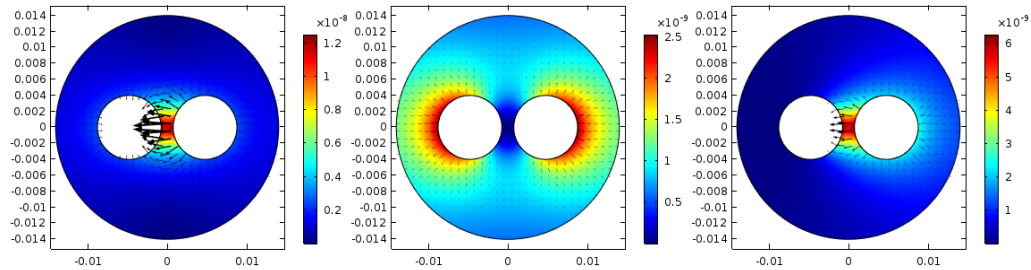


Fig. 10. Electric displacement field in cases 1–3 from left to right with  $d_c$  of 9.5 mm ( $C/m^2$ )

Table 1. Results of numerical calculations with  $d_c$  of 9.5 mm

Case/Method	Energy	Field	Charge	Average
Unit	pF/m	pF/m	pF/m	pF/m
C1	53.607	53.601	53.607	53.605
C2	76.701	78.721	76.703	77.375
C3	72.784	72.777	72.777	72.779

match and the formulas hold. The results of numerical calculations in the range of  $d_c$  from 8.2 to 14 mm and experimental results normalized to vacuum are presented in Figure 11. The numerical results are represented as solid lines, while experimental results are shown as markers. The vertical lines represent the separations in which respective experimental measurements were performed. The results obtained by the oscilloscope method from [9] are also presented.

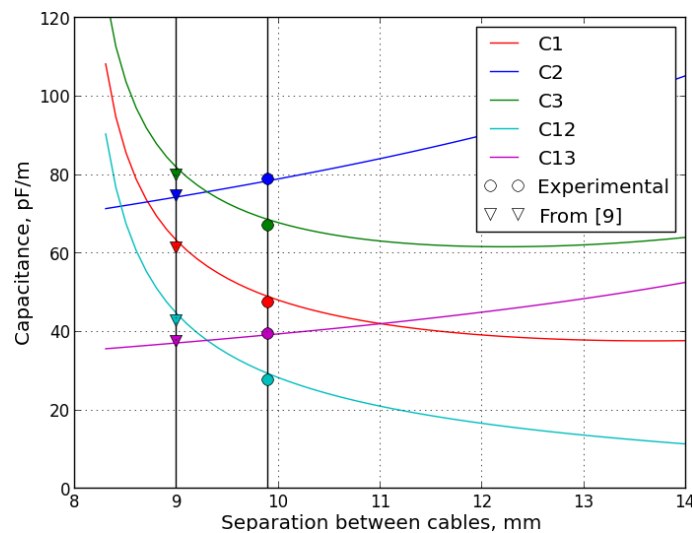


Fig. 11. Comparison between numerical and experimental results as the function of  $d_c$

Table 2 contains the values of the experimental results performed at specific separations between cables (9 mm for the data from [9] and 9.9 mm for our results). The percentage difference between the model and experimental results is calculated.

Table 2. Results of comparison between numerical and experimental results

Separation	9 mm [from 9 – oscilloscope method]			9.9 mm			
	Value	Numerical	Measured	Discrepancy	Numerical	Measured	Discrepancy
Unit	pF/m	pF/m	pF/m	%	pF/m	pF/m	%
C1	63.22	61.35	61.35	-2.96	48.99	47.49	-3.06
C2	74.42	74.42	74.70	0.37	78.56	78.84	0.36
C3	81.83	81.83	80.02	-2.20	68.63	67.20	-2.08
C12	44.61	44.61	42.67	-4.35	29.35	27.78	-5.35
C13	37.21	37.21	37.35	0.37	39.28	39.42	0.36

Small discrepancy is observed. It can be caused by the erroneous placement of the cables in the tube. The other source of discrepancies can be the effect of the ends of the cable outside of the shielding pipe. The end effects were not considered in numerical calculations. In the case of the considered accelerator the dominant input to the total capacity of the lines is that of long straight fragments. In the scale of the entire device, input from the ends can be neglected without significant loss of accuracy.

Another possible cause can be the fact that the measurements were performed in air at the room temperature leading to erroneous assumption of the material parameters in the model, especially permittivity. In spite of these problems the experimental values obtained by us are close to the experimental and prove the numerical model to be a good tool to quickly estimate the unit capacitance of the line in wide range of possible line geometries.

#### 4. Conclusion

The unit capacitance of the superconducting bus-bar line is found. Values obtained with the numerical calculations are consistent with each other, no matter which method was used. Small discrepancy exists between the experiment and numerical calculations. The difference can be explained by non-ideal conditions of the experiment – finite length of the sample and change of properties between liquid nitrogen temperature and liquid helium temperature. Despite that the values obtained both experimentally and numerically are within the required limits of the accelerator.

#### Acknowledgements

This work has received funding from Ministry for Science and Higher Education under FAIR in-kind Contract between Facility for Antiproton and Ion Research in Europe GmbH, Jagiellonian University and Wrocław University of Science and Technology.

The authors are grateful to Wrocław Networking and Supercomputing Center for granting access to the computing infrastructure.

The authors are grateful to Mr Maciej Cholewiński for the help in the preparation of drawings.

## References

- [1] Outeiro M.T., Visintini R., Buja G., *Considerations in designing power supplies for particle accelerators*, IECON 2013 – 39-th Annual Conference of the IEEE, Industrial Electronics Society, 2013, DOI: 10.1109/IECON.2013.6700307.
- [2] Bertarelli A., *Beam-induced damage mechanisms and their calculation*, CERN Yellow Reports, vol. 2, no. 0, p. 159 (2016).
- [3] Kahle K., *Power Converters and Power Quality*, Proceedings of the CAS-CERN Accelerator School: Power Converters (2015).
- [4] Eisel T., Chorowski M., Iluk A., Kauschke M., Kollmus H., Malcher K., Poliński J., Streicher B., *Local Cryogenics for the SIS100 at FAIR*, IOP Conference Series: Materials Science and Engineering, vol. 101, 2015, DOI: 10.1088/1757-899X/101/1/012075.
- [5] Tomków Ł., Trojanowski S., Cizek M., Chorowski M., *Heat generation by eddy currents in a shell of superconducting bus-bars for SIS100 particle accelerator at FAIR*, Archives of Electrical Engineering, vol. 66, no. 4, pp. 705–715 (2017).
- [6] FAIR collaboration, *FAIR Baseline Technical Report*, vol. 1, March (2006).
- [7] Stafiniak A., Szwangruber P., Freisleben W., Floch E., *Electrical integrity and its protection for reliable operation of superconducting machines*, Physics Procedia, vol. 67, pp. 1106–1111 (2015).
- [8] Trojanowski S., Cizek M., Chorowski M., *Measurements of capacitances and self-inductances of lines supplying superconducting magnets (project FAIR)*, Wrocław University of Technology (in Polish, unpublished) (2015).
- [9] Sanchez A.V., Plyusnin V., *Measurement of Bus Bars capacitances*, GSI Note (unpublished) (2015).